universe

IMPACT FACTOR 2.6

CITESCORE 5.2

Article

Measurement of Ion Mobilities for the Ion-TPC of NvDEx Experiment

Tianyu Liang, Meiqiang Zhan, Hulin Wang, Xianglun Wei, Dongliang Zhang, Jun Liu, Chengui Lu, Qiang Hu, Yichen Yang, Chaosong Gao et al.

Special Issue

Exploring Double Beta Decay: Probing Fundamental Properties of Neutrinos and Beyond

Edited by

Prof. Dr. Rita Bernabei

MDPI

https://doi.org/10.3390/universe11050163

universe

MDPI

Article

Measurement of Ion Mobilities for the Ion-TPC of NvDEx Experiment

Tianyu Liang [1], Meiqiang Zhan [2], Hulin Wang [1,*], Xianglun Wei [3], Dongliang Zhang [1], Jun Liu [1], Chengui Lu [3,*], Qiang Hu [3], Yichen Yang [3], Chaosong Gao [1], Le Xiao [1], Xiangming Sun [1], Feng Liu [1], Chengxin Zhao [3], Hao Qiu [3] and Kai Chen [1,*]

[1] PLAC, Key Laboratory of Quark & Lepton Physics (MOE), Central China Normal University, 152 Luoyu Rd., Wuhan 430079, China; tianu.liang@mails.ccnu.edu.cn (T.L.)
[2] Institute of Nuclear Science and Technology, Sichuan University, 29 Wangjiang Rd., Chengdu 610065, China
[3] Institute of Modern Physics, Chinese Academy of Sciences, 509 Nanchang Rd., Lanzhou 730000, China
* Correspondence: hulin.wang@ccnu.edu.cn (H.W.); luchengui@impcas.ac.cn (C.L.); chenkai@ccnu.edu.cn (K.C.)

Abstract: In the NνDEx collaboration, a high-pressure gas TPC is being developed to search for the neutrinoless double beta decay. The use of electronegative $^{82}SeF_6$ gas mandates an ion-TPC. The reconstruction of the z coordinate is to be realized by exploiting the feature of multiple species of charge carriers. As the initial stage of the development, we studied the properties of the SF_6 gas, which is non-toxic and has a similar molecular structure to SeF_6. In the paper, we present the measurement of drift velocities and mobilities of the majority and minority negative charge carriers found in SF_6 at a pressure of 750 Torr, slightly higher than the local atmospheric pressure. The reduced fields range between 3.0 and 5.5 Td. This was performed using a laser beam to ionize the gas inside a small TPC, with a drift length of 3.7 cm. A customized charge-sensitive amplifier was developed to read out the anode signals induced by the slowly drifting ions. The closure test of the reconstruction of the z coordinate using the difference in the velocities of the two carriers was also demonstrated.

Keywords: double beta decay detectors; gaseous imaging and tracking detectors; Time projection chambers (TPC); charge transport and multiplication in gas

check for updates

Academic Editor: Rita Bernabei

Received: 9 April 2025
Revised: 12 May 2025
Accepted: 15 May 2025
Published: 16 May 2025

Citation: Liang, T.; Zhan, M.; Wang, H.; Wei, X.; Zhang, D.; Liu, J.; Lu, C.; Hu, Q.; Yang, Y.; Gao, C.; et al. Measurement of Ion Mobilities for the Ion-TPC of NvDEx Experiment. *Universe* **2025**, *11*, 163. https://doi.org/10.3390/universe11050163

Copyright: © 2025 by the authors. Licensee MDPI, Basel, Switzerland. This article is an open access article distributed under the terms and conditions of the Creative Commons Attribution (CC BY) license (https://creativecommons.org/licenses/by/4.0/).

1. Introduction

The search for neutrinoless double beta decay ($0\nu\beta\beta$) is an ideal way to probe the Majorana nature of the neutrinos. In addition, its discovery will prove that the lepton number is not conserved and help to study the absolute masses of the neutrinos and their origin. Recent or future experiments worldwide search for $0\nu\beta\beta$ decay using diverse technologies, including high-purity germanium detectors (GERDA [1], MAJORANA DEMONSTRATOR [2], LEGEND [3], CDEX [4]), time-projection chambers (TPCs) with Xe (EXO-200 [5], nEXO [6], NEXT [7], PandaX-III [8], LZ [9], DARWIN [10]), liquid scintillators (KamLAND-Zen [11], SNO+ [12]), cryogenic calorimeters (CUORE [13], CUPID [14], CROSS [15], AMoRE [16]), and tracking calorimeters (NEMO-3 [17], SuperNEMO [18]).

The NνDEx collaboration [19] proposed to search for $0\nu\beta\beta$ decay of ^{82}Se using a high-pressure $^{82}SeF_6$ gas TPC [20]. The SeF_6 has a high electron affinity, and the electrons produced by the ionization process are quickly captured by the SeF_6 molecules to form negative ions. The negative ions are to be collected by the readout plane [21,22], consisting of CMOS integrated charge sensors named Topmetal-S [23], without being amplified in the gas. The main feature of Topmetal-S is its exposed metal on the top layer of the chip

to sense the drifting charge carriers in the gas, hence integrating the functions of both the charge sensor and the readout application-specific integrated circuit in one chip. With this design, low noise can be realized, which is important for direct sensing. Both negative and positive ions are envisaged to be detected by the charge sensors, while in the first phase of the experiment with 100 kg $^{82}SeF_6$ at 10 bar [19], only negative ions will be probed.

It is expected that in SeF_6, the negative ions are predominantly SeF_5^- and SeF_6^-, like in SF_6, which has a similar molecular structure. One advantage is that, by using the different drift velocities of the two charge carriers, the z coordinate can be calculated without the need for a start time, which is difficult to implement in the NνDEx experiment. The SeF_6 is toxic and needs to be handled with care. So in the first phase of the gas property study for the NνDEx experiment, we begin by studying SF_6 gas. The properties of SF_6 have been studied in a low-pressure environment [24] for dark matter experiments. In our study, we aim to observe and measure the properties of SF_5^- and SF_6^- at atmospheric pressure and to study the z coordinate reconstruction.

The paper is structured as follows. The experimental apparatus and the method are described in Section 2. The results of the measurements, including the waveforms, velocities, and mobilities, are presented in Section 3. The reconstruction of the z coordinate using the different drift velocities of the two charge carriers is demonstrated in Section 4, followed by the conclusion in Section 5.

2. Experimental Apparatus and Method

2.1. Device Setup

The overall device setup for the measurement is shown in Figure 1. A Quantel Q-smart (450 mJ) laser is used to generate a pulsed laser beam with a wavelength of 266 nm. It also sends a trigger signal, which marks the start time of the event. The laser beam ionizes the gas in the TPC, and the anode plane below the grid is used to collect the negative ions. The anode plane is connected to a charge-sensitive amplifier (CSA), which turns the current signal into a voltage signal. Both the trigger signal and the signal from the CSA are sent to a Tektronix MSO5034B oscilloscope for further analyses. The high voltages of the TPC are provided by the iseg EHS 80-60n module.

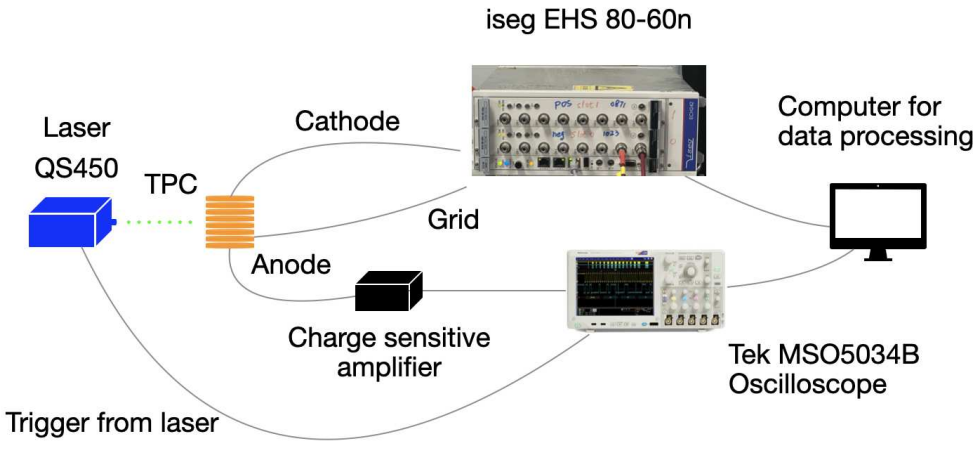

Figure 1. The overall device setup.

The photo of the laser and the steel gas vessel is shown in Figure 2 (left). The laser beam enters the field cage of the TPC through a quartz window in the gas vessel. The photo of the field cage inside the gas vessel is shown in Figure 2 (right). It has a length of 40 mm, and the maximum drift distance (between the cathode and the grid) is 38 mm. The grid is made of wires with a diameter of 50 µm, and there is a 2 mm gap between the grid and the

anode. The field rings are made of 2 mm wide copper strips at a pitch of 4 mm. They are connected by the 10 MΩ resistors.

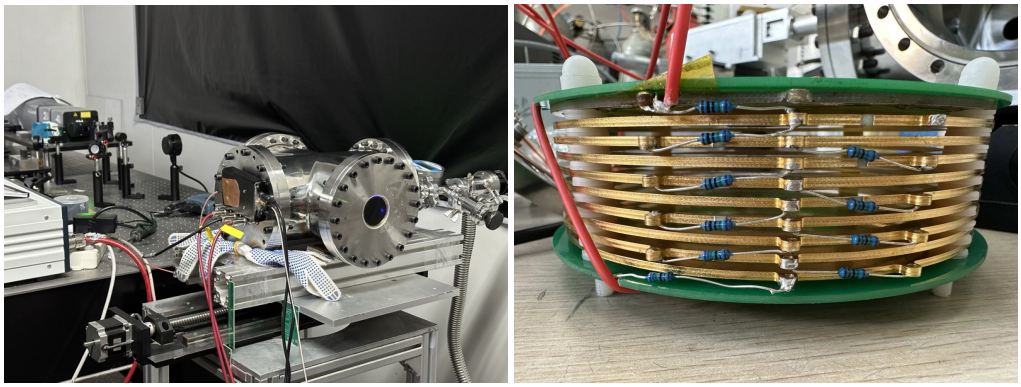

Figure 2. The photo of the laser and the gas vessel (**left**) and the photo of the field cage (**right**).

2.2. The CSA

To detect the signal induced by the slowly drifting ions, a CSA has been specifically developed for the measurement, with its structure and photo shown in Figure 3.

It has two amplification stages. The current signal from the anode plane passes through the blocking capacitor C_1 and then enters the first amplification stage, which is composed of a transistor and an OPA211 [25] amplifier chip. A JFET 2N4416 is used for its small gate leakage current and high transconductance. The resistors R_1, R_2, and R_3 are used to adjust the quiescent point of the JFET to make it work in the amplification regime. The decay time constant of the CSA is determined by the product of the feedback resistor R_f and the feedback capacitor C_f. The C_2 and R_4 form a high-pass filter. The output of the first stage is filtered and then enters the second amplification stage with another OPA211 chip, with the gain determined by R_6/R_5. The output impedance is 50 Ω. A test pulse could be injected into the TESTIN pin to calibrate the CSA with the injection capacitance C_{inj}.

The values of C_f and R_f were adjusted to achieve the desired decay time constant and noise performance of the CSA. In the subsequent measurements, 50 fF and 1 GΩ were adopted for C_f and R_f, respectively. The main reason for the rather short 50 μs decay time constant was to avoid the saturation of the CSA during the measurement, which will be improved to allow longer decay time in the future.

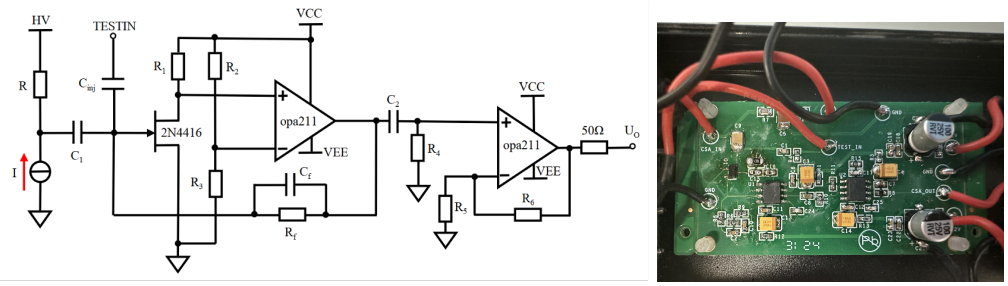

Figure 3. The structure (**left**) and photo (**right**) of the CSA used in the measurement.

3. Results of Measurement

3.1. Waveforms of SF_6

The laser beam, with a diameter of about 1 mm, enters the field cage through a 2 mm wide gap below the cathode. The laser beam is parallel to the cathode, and the distance between the beam center and the grid is 37 mm, which defines the drift length of the measurement. The trigger signal from the laser gives the start time of the event. The gas pressure is 750 Torr, slightly higher than the local atmospheric pressure of 630 Torr. The

measurement was carried out at a room temperature of about 20 °C. The electric field strength of the drift region varies between 735 V/cm and 1351 V/cm. The electric field strength between the grid and the anode is fixed at 5000 V/cm.

The waveforms of the voltage signals from the CSA are acquired by the oscilloscope. The rise time of the CSA is about 1 µs, which is three orders of magnitude smaller than the typical time scale of the signal development. Therefore, the current signal is calculated from the voltage signal using the equation [24]:

$$I(t) \propto \frac{dV}{dt} - (-\frac{V}{\tau}) \tag{1}$$

where τ is the decay time constant of the CSA. The current waveforms are then smoothed with a Butterworth filter to suppress high-frequency noise.

Figures 4 and 5 show the typical waveforms of the voltage signals and the resulting current signals, respectively. It is estimated that approximately 3 M to 10 M negative ions were collected per laser beam. The trigger signals from the laser are also shown in the voltage waveforms. Due to the small decay time of CSA, the waveform of the current signal is similar to the corresponding waveform of the voltage signal. For the current waveforms, the amplitudes of the majority of the peaks are normalized to the unit.

Due to the small drift length and finite laser beam width, the waveforms of the two charge carriers are not quite separated from each other. But it can indeed be seen that there are at least two charge carriers in the current waveform, and the minority peak becomes more obvious for a higher drift field. The minority charge carrier, and the faster one, is postulated to be SF_5^-, while the majority charge carrier, and the slower one, is postulated to be SF_6^-. There is also a long tail on the right side of the majority peak. This could be due to $SF_5^-(SF_6)_n$ and $SF_6^-(SF_6)_n$, as well as $SF_6^-(H_2O)_n$, which drifts at a slower speed than the SF_6^-.

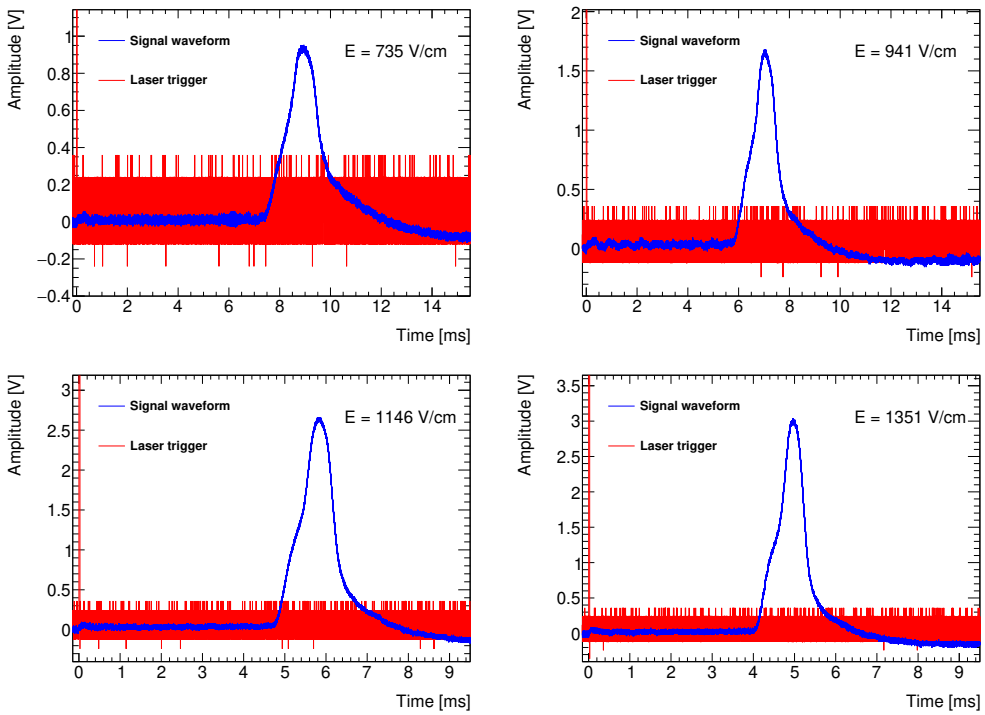

Figure 4. The typical waveforms of the voltage signals, for four drift fields between 735 V/cm and 1351 V/cm. The trigger signals from the laser are also shown.

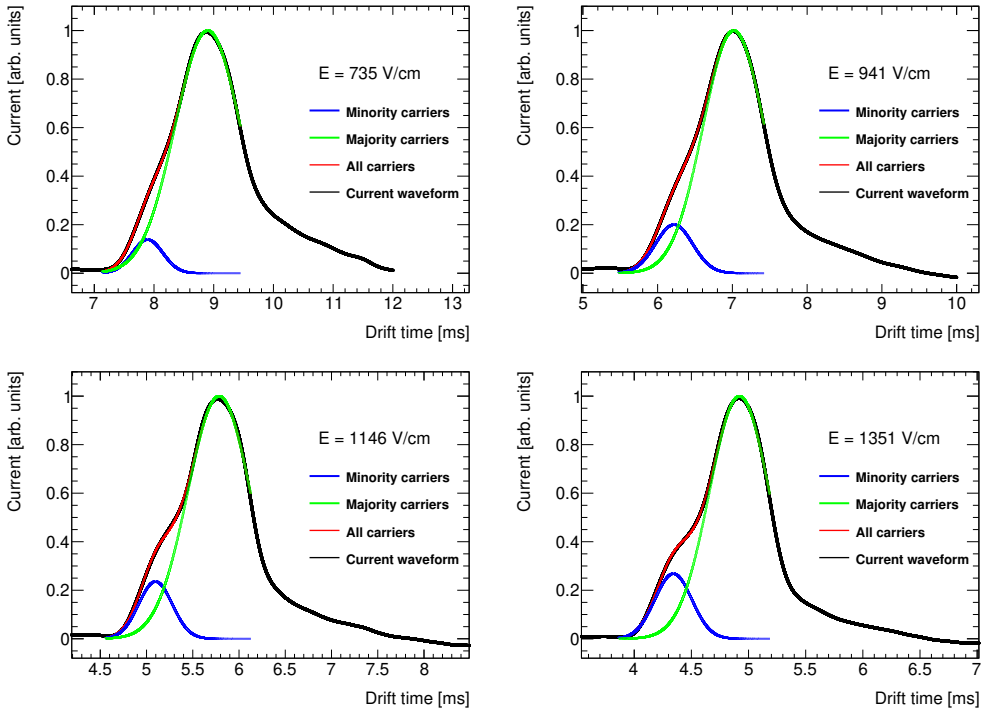

Figure 5. The typical waveforms of the current signals, converted from the voltage waveforms using Equation (1), are shown for four drift fields between 735 V/cm and 1351 V/cm. The amplitude of the majority peak is normalized to unity. The double-Gaussian fit to each waveform is also shown to extract the separate drift times of the minority and majority charge carriers.

The ratio of the amplitude of the minority carrier to that of the majority carrier increases from 0.13 to 0.28 as the drift field increases from 735 V/cm to 1351 V/cm. These are larger than the values reported in the measurement at low pressure [24]. We suspect that it is mainly due to the different signal generation mechanisms, i.e., we use a laser beam to ionize the gas. The cross section of SF_5^- has a strong dependence on the electron energy and could be enhanced in our case. The relative amplitude between SF_5^- and SF_6^- under different conditions will be further studied in the next step.

3.2. Drift Velocities and Mobilities

The drift times of SF_5^- and SF_6^- are extracted by fitting a double-Gaussian function to the current waveform to extract their separate contributions, and the two μ values are used as their drift times. Examples of the double-Gaussian fit are shown in Figure 5 for four different drift fields. Due to the long tail on the right side of the majority peak, as explained in Section 2.2, the range of the fit is only up to about one standard deviation above the majority peak. The distributions of drift times for SF_5^- and SF_6^- are shown in Figure 6, for four different drift fields.

The drift velocity v_d is then calculated as the ratio between the 37 mm drift distance and the drift time. A total of 1.5 mm systematic uncertainty is considered on the drift length, including a ∼1 mm uncertainty for the position and width of the laser beam, and a ∼0.5 mm uncertainty for the impact of a 2 mm gap between the grid and anode at 5000 V/cm. Figure 7 (left) shows the drift velocities of SF_5^- and SF_6^- as a function of the drift field.

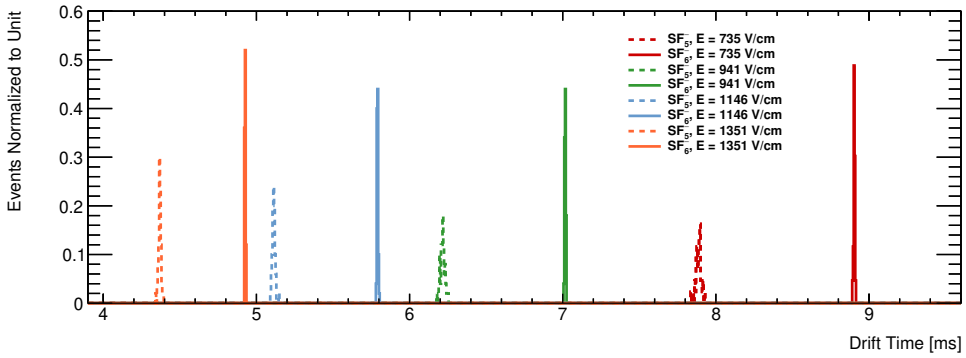

Figure 6. The distributions of drift times for SF_5^- and SF_6^-, for four drift fields between 735 V/cm and 1351 V/cm.

The reduced mobility μ_0 is also calculated, defined as:

$$\mu_0 = \frac{v_d}{E}\frac{N}{N_0} \tag{2}$$

where $N_0 = 2.687 \times 10^{19}$ cm^{-3} is the gas density at STP (°C and 760 Torr). A conservative 1% uncertainty is considered on the pressure and temperature, taking into account the <1 °C variation and 1 °C accuracy of the temperature measurement, and the <0.1 mbar variation and 0.1% accuracy of the pressure measurement. Figure 7 (right) shows the reduced mobilities of SF_5^- and SF_6^- as a function of the reduced field E/N in Townsend units (1 Td = 10^{-17} Vcm^2).

The reduced fields range between 3.0 and 5.5 Td. The reduced mobilities of SF_5^- vary between 0.576 ± 0.024 cm^{2}V^{-1}s^{-1} and 0.587 ± 0.025 cm^{2}V^{-1}s^{-1}, while the reduced mobilities of SF_6^- vary between 0.511 ± 0.021 cm^{2}V^{-1}s^{-1} and 0.520 ± 0.022 cm^{2}V^{-1}s^{-1}. The values are consistent with what was reported in Ref. [24] under the uncertainties.

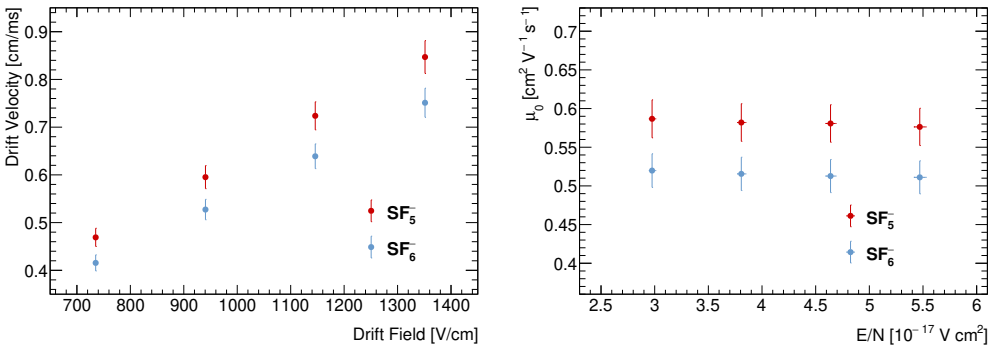

Figure 7. The drift velocities (**left**) and reduced mobilities (**right**) of SF_5^- and SF_6^-.

4. Reconstruction of z Coordinate

Without using the start time, the z coordinate could be reconstructed by using the difference in the arrival times of SF_5^- and SF_6^-, and their pre-calibrated drift velocities. The z coordinate reconstruction is demonstrated using the same datasets of Section 3, following the equation:

$$z = \frac{v_{SF_5^-} \cdot v_{SF_6^-}}{v_{SF_5^-} - v_{SF_6^-}} \cdot \Delta t \tag{3}$$

where Δt is the difference in the arrival times of SF_5^- and SF_6^- in each event, while $v_{SF_5^-}$ and $v_{SF_6^-}$ are the measured drift velocities in Section 3.2.

Figure 8 shows the distributions of the reconstructed z-coordinate of the laser beam for four drift fields between 735 V/cm and 1351 V/cm. For each drift field, half (∼50) of the laser pulses are used to calculate the drift velocities, and the other half is used for the z-coordinate reconstruction. The means of distributions range from 3.699 to 3.702 cm as expected, with the standard deviations varying from 0.046 to 0.069 cm. Figure 8 provides a closure test of the velocity measurements and z coordinate reconstruction.

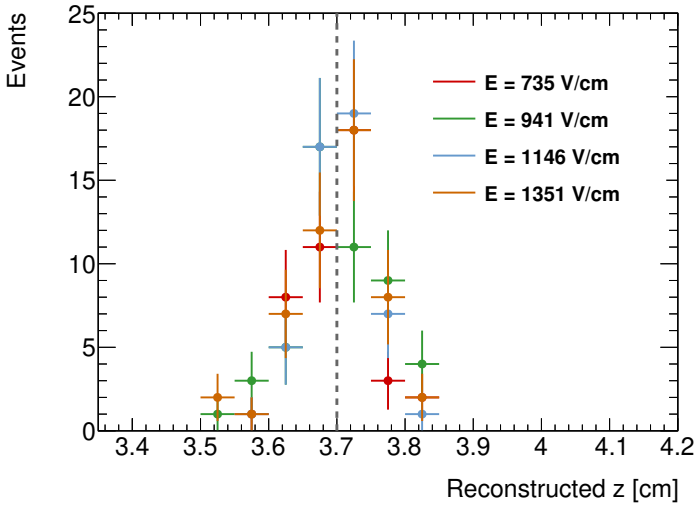

Figure 8. The distributions of the reconstructed z-coordinate of the laser beam for four drift fields between 735 V/cm and 1351 V/cm.

5. Conclusions

For the first phase of the gas property study for the NνDEx experiment using high-pressure $^{82}SeF_6$ gas TPC to search for $0\nu\beta\beta$ decay, a structurally similar SF_6 gas was examined at 750 Torr and room temperature, with the drift fields ranging from 735 V/cm to 1351 V/cm. The corresponding reduced fields range from 3.0 to 5.5 Td.

The minority charge carrier SF_5^- and the majority charge carrier SF_6^- were observed in the waveforms, and their drift velocities and mobilities were measured using a small TPC and a custom-developed CSA. The signals were generated by ionizing the gas using a laser beam.

A closure test of the reconstruction of the z coordinate using the difference in the arrival times of the two negative ion species was successfully performed.

The work in the paper lays the groundwork for future studies on the properties of $^{82}SeF_6$ gas. Measurements will be improved and extended to higher pressures close to the value in the NνDEx experiment, to positive ions, and to other gas properties including diffusion, W value, and the Fano factors.

Author Contributions: Conceptualization, H.W., K.C. and C.L.; methodology, H.W. and T.L.; software, H.W. and T.L.; validation, M.Z., T.L. and C.L.; formal analysis, T.L., M.Z. and H.W.; investigation, T.L.; resources, Q.H., C.L., X.W., C.G. and J.L.; data curation, C.L., M.Z. and T.L.; writing—original draft preparation, H.W., J.L. and T.L.; writing—review and editing, D.Z., H.W. and T.L.; visualization, F.L., D.Z., Y.Y. and X.S.; supervision, X.S., H.Q., L.X. and C.Z.; project administration, H.W. and K.C.; funding acquisition, H.W. All authors have read and agreed to the published version of the manuscript.

Funding: This research was funded by the National Natural Science Foundation of China under Grant 12105110, and in part by the National Key Research and Development Program of China under Grant 2022YFA1604703, 2021YFA1601300.

Data Availability Statement: The original data presented in the study are openly available in FigShare at 10.6084/m9.figshare.29085428.

Acknowledgments: The authors gratefully acknowledge the support from the Key Laboratory of Quark & Lepton Physics (MOE), Central China Normal University, and the Nuclear Detection Technology and Experiment Platform Center, Institute of Modern Physics, Chinese Academy of Sciences.

Conflicts of Interest: The authors declare no conflicts of interest.

References

1. Agostini, M. et al. [GERDA Collaboration]. Upgrade for phase ii of the gerda experiment. *Eur. Phys. J. C* **2018**, *78*, 388. [CrossRef]
2. Abgrall, N. et al. [Majorana Collaboration]. The majorana demonstrator neutrinoless double-beta decay experiment. *Adv. High Energy Phys.* **2014**, *2014*, 365432. [CrossRef]
3. Abgrall, N. et al. [LEGEND Collaboration]. Legend-1000 preconceptual design report. *arXiv* **2021**, arXiv:2107.11462.
4. Wang, L.; Yue, Q.; Kang, K.; Cheng, J.; Li, Y.; Wong, T.H.; Lin, S.; Chang, J.; Chen, J.; Chen, Q.; et al. First results on ^{76}Ge neutrinoless double beta decay from CDEX-1 experiment. *Sci. China Phys. Mech. Astron.* **2017**, *60*, 071011. [CrossRef]
5. Auger, M.; Auty, D.J.; Barbeau, P.S.; Bartoszek, L.; Baussan, E.; Beauchamp, E.; Benitez-Medina, C.; Breidenbach, M.; Chauhan, D.; Cleveland, B.; et al. The EXO-200 detector, part i: Detector design and construction. *J. Instrum.* **2012**, *7*, P05010. [CrossRef]
6. Adhikari, G.; Al Kharusi, S.; Angelico, E.; Anton, G.; Arnquist, I.J.; Badhrees, I.; Bane, J.; Belov, V.; Bernard, E.P.; Bhatta, T.; et al. nEXO: Neutrinoless double beta decay search beyond 10^{28} year half-life sensitivity. *J. Phys. G Nucl. Part. Phys.* **2021**, *49*, 015104. [CrossRef]
7. Novella, P. et al. [The NEXT Collaboration]. Demonstration of neutrinoless double beta decay searches in gaseous xenon with NEXT. *J. High Energy Phys.* **2023**, *2023*, 190. [CrossRef]
8. Chen, X.; Fu, C.; Giboni, K.; Giuliani, F.; Gu, L.; Han, K.; Ji, X.; Lin, H.; Liu, J.; Ni, K.; et al. PandaX-III: Searching for neutrinoless double beta decay with high pressure ^{136}Xe gas time projection chambers. *Sci. China Phys. Mech. Astron.* **2017**, *60*, 061011. [CrossRef]
9. Akerib, D.S. et al. [LZ Collaboration]. Lux-zeplin (lz) conceptual design report. *arXiv* **2015**, arXiv:1509.02910.
10. Aalbers, J.; Agostini, F.; Alfonsi, M.; Amaro, F.; Amsler, C.; Aprile, E.; Arazi, L.; Arneodo, F.; Barrow, P.; Baudis, L.; et al. DARWIN: Towards the ultimate dark matter detector. *J. Cosmol. Astropart. Phys.* **2016**, *2016*, 017. [CrossRef]
11. Abe, S. et al. [KamLAND-Zen Collaboration]. Search for the majorana nature of neutrinos in the inverted mass ordering region with kamland-zen. *Phys. Rev. Lett.* **2023**, *130*, 051801. [CrossRef] [PubMed]
12. Albanese, V. et al. [The SNO+ Collaboration]. The SNO+ experiment. *J. Instrum.* **2021**, *16*, P08059. [CrossRef]
13. Alduino, C.; Alessandria, F.; Balata, M.; Biare, D.; Biassoni, M.; Bucci, C.; Caminata, A.; Canonica, L.; Cappelli, L.; Ceruti, G.; et al. The CUORE cryostat: An infrastructure for rare event searches at millikelvin temperatures. *Cryogenics* **2019**, *102*, 9–21. [CrossRef]
14. CUPID Interest Group. Cupid pre-CDR. *arXiv* **2019**, arXiv:1907.09376.
15. Bandac, I.C. et al. [The CROSS Collaboration]. The $0\nu2\beta$-decay cross experiment: Preliminary results and prospects. *J. High Energy Phys.* **2020**, *2020*, 18. [CrossRef]
16. Lee, M. AMoRE: A search for neutrinoless double-beta decay of ^{100}Mo using low-temperature molybdenum-containing crystal detectors. *J. Instrum.* **2020**, *15*, C08010. [CrossRef]
17. Arnold, R. et al. [NEMO-3 Collaboration]. Results of the search for neutrinoless double-β decay in ^{100}Mo with the nemo-3 experiment. *Phys. Rev. D* **2015**, *92*, 072011. [CrossRef]
18. Piquemal, F. The SuperNEMO project. *Phys. At. Nucl.* **2006**, *69*, 2096–2100. [CrossRef]
19. Cao, X.-G.; Chang, Y.-L.; Chen, K.; Ciuffoli, E.; Duan, L.-M.; Fang, D.-L.; Gao, C.-S.; Ghorui, S.K.; Hu, P.-C.; Hu, Q.; et al. NνDEx-100 conceptual design report. *Nucl. Sci. Tech.* **2023**, *35*, 3. [CrossRef]
20. Nygren, D.; Jones, B.; López-March, N.; Mei, Y.; Psihas, F.; Renner, J. Neutrinoless double beta decay with $^{82}SeF_6$ and direct ion imaging. *J. Instrum.* **2018**, *13*, P03015. [CrossRef]
21. Lang, L.; Hu, Y.; Yu, Z.; You, B.; Liang, T.; He, Z.; Liu, J.; Huang, G.; Wang, H.; Xiao, L.; et al. Design and demonstration of digital readout chain in NνDEx experiment. *IEEE Trans. Nucl. Sci.* **2023**, *70*, 2499–2505. [CrossRef]
22. Yang, Y.; Liang, T.; Gao, C.; Zhang, D.; Chen, K.; Wang, H.; Liu, J.; Liu, L.; Qiao, Y.; Hu, Z.; et al. Design and preliminary test results of the charge sensitive amplifier for gain-less charge readout in high-pressure TPC. *J. Instrum.* **2024**, *19*, C03031. [CrossRef]
23. Liang, T.; Zhang, D.; Wang, H.; Gao, C.; Liu, J.; Sun, X.; Xiao, L.; Liu, F.; You, B.; Liu, L.; et al. Performance of a novel charge sensor on the ion detection for the development of a high-pressure avalancheless ion TPC. *J. Instrum.* **2024**, *19*, C04004. [CrossRef]

24. Phan, N.; Lafler, R.; Lauer, R.; Lee, E.; Loomba, D.; Matthews, J.; Miller, E. The novel properties of SF_6 for directional dark matter experiments. *J. Instrum.* **2017**, *12*, P02012. [CrossRef]
25. Texas Instruments. OPA211: Ultra-Low Noise, Precision Operational Amplifier; Data Sheet, Document Number: SBOS377M. 2022. Available online: https://www.ti.com/lit/ds/symlink/opa211.pdf (accessed on 10 May 2025).

Disclaimer/Publisher's Note: The statements, opinions and data contained in all publications are solely those of the individual author(s) and contributor(s) and not of MDPI and/or the editor(s). MDPI and/or the editor(s) disclaim responsibility for any injury to people or property resulting from any ideas, methods, instructions or products referred to in the content.